Potential-well depth at amorphous-$LaAlO_3$/crystalline-$SrTiO_3$ interfaces measured by optical second harmonic generation

Gabriele De Luca,[a] Andrea Rubano, Emiliano di Gennaro, Amit Khare, Fabio Miletto Granozio, Umberto Scotti di Uccio, Lorenzo Marrucci, and Domenico Paparo[b]
CNR-SPIN and Dipartimento di Fisica, Università di Napoli "Federico II," Compl. Univ. di Monte S. Angelo, v. Cintia, 80126 Napoli, Italy

(Received 25 February 2014; accepted 20 June 2014; published online 1 July 2014)

By a combination of optical second harmonic generation and transport measurements, we have investigated interfaces formed by either crystalline or amorphous thin films of $LaAlO_3$ grown on TiO_2-terminated $SrTiO_3$(001) substrates. Our approach aims at disentangling the relative role of intrinsic and extrinsic doping mechanisms in the formation of the two-dimensional electron gas. The different nature of the two mechanisms is revealed when comparing the sample response variation as a function of temperature during annealing in air. However, before the thermal treatment, the two types of interfaces show almost the same intensity of the second harmonic signal, provided the overlayer thickness is the same. As we will show, the second harmonic signal is proportional to the depth of the potential well confining the charges at the interface. Therefore, our result demonstrates that this depth is about the same for the two different material systems. This conclusion supports the idea that the electronic properties of the two-dimensional electron gas are almost independent of the doping mechanism of the quantum well. © *2014 AIP Publishing LLC*.
[http://dx.doi.org/10.1063/1.4886413]

Since the discovery of a two-dimensional electron gas (2DEG) formed at the interface between the two band insulators $LaAlO_3$ (LAO) and $SrTiO_3$ (STO),[1] a worldwide research effort has unveiled a surprising array of unexpected phenomena in this material system, ranging from tunable conductivity to two-dimensional superconductivity.[2]

The origin of the charge carriers immediately emerged as a highly debated question, since different doping mechanisms can be at play in this oxide heterostructure. A large body of evidence points to the so-called *polar catastrophe* scenario as the mechanism driving the formation of the conducting state.[3–7] According to this picture, electrons are transferred from the surface to the interface to compensate the built-in potential within the polar LAO film.

However, many experimental observations have highlighted the presence of point defects, such as cationic intermixing across the interface or oxygen vacancies, able to introduce a chemical doping even in absence of electronic reconstruction.[3,8–11] Recently, the oxygen-vacancy mechanism has attracted a renewed attention because of the observation that a two-dimensional gas is formed at LAO/STO interfaces even when the LAO film is grown in amorphous phase, so as to rule out polar-discontinuity-related mechanisms.[12–15]

In the following, we indicate the amorphous structure as *a*-LAO/STO in order to distinguish it from the crystalline, *c*-LAO/STO, structure. These two types of interfaces are investigated here by resorting to optical second harmonic generation (SHG), a technique which recently has been applied to studying *c*-LAO/STO interfaces.[16–22]

In SHG, an optical wave with frequency 2ω is generated from an incident wave of frequency ω. For this process to occur, a breaking of the material inversion symmetry is needed. The latter naturally takes place at the interface between two dissimilar centrosymmetric media, such as LAO and STO within the temperature range considered in this work. Additionally, the inversion symmetry can be broken in the bulk of centrosymmetric media because of the presence of a bias static electric field, $\boldsymbol{E}^{polar}$.[23] The actual measured quantity is the SHG intensity I_{SHG}, which is proportional to the square of the reflected SHG optical field: $I_{SHG} \propto |E_{SHG}|^2$. The latter is, in turn, proportional to the square of the incident optical field, $E_{SHG} \propto \chi^{\text{eff}} E_0^2$, where χ^{eff} is in general defined as follows:[26]

$$\chi^{\text{eff}}_{\text{in,out}} = \int e_i^{\text{out}} [\chi^{(2)}_{ijk}(z) + \chi^{(3)}_{ijkl}(z) E_l^{polar}(0,z)] e_j^{\text{in}} e_k^{\text{in}} dz, \qquad (1)$$

where z is the coordinate along the surface normal and $\mathbf{e}^{\text{in, out}}$ are the optical polarization unit vectors in vacuum of the input and output waves, respectively.[24] In Eq. (1), $\chi^{(2)}_{ijk}$ and $\chi^{(3)}_{ijkl}$ denote the second- and third-order susceptibility tensors, respectively. The first term takes into account the structural symmetry breaking occurring at the interface between two dissimilar media. The second term describes the symmetry breaking caused by a bias static field in the region of the quantum well, as depicted in Figs. 4(b) and 4(c) and better explained in the following.

In Eq. (1), the z integral is extended across the entire thickness of the polar layer, d_{polar}, where the inversion symmetry is broken. d_{polar} is assumed to be much thinner than the optical wavelength. Under the dipole approximation, the bulk of *c*-LAO, *c*-STO, and *a*-LAO do not contribute to $\chi^{(2)}$ since they are centrosymmetric, while their interfaces, LAO/STO and LAO/air, do. Additionally, any region of the LAO/STO

[a]Present address: Department of Materials, ETH Zurich, Wolfgang-Pauli-Strasse 10, 8093 Zurich, Switzerland.
[b]Electronic mail: domenico.paparo@spin.cnr.it

heterostructure may become SHG active, through $\chi^{(3)}$, if exposed to a bias electric field. However, in our past work on *c*-LAO/STO interfaces, we have clearly demonstrated that, at the wavelength used in this experiment, the SHG signal originates principally in a very thin layer of STO close to the interface.[22] This fact demonstrates that $\chi^{(2)}_{ijk}$ of the LAO/air interface as well as $\chi^{(3)}$ of the LAO bulk are negligibly small. Therefore, from here on, d_{polar} identifies the thickness of a very thin layer of STO close to the interface, in the region of quantum well.

LAO/STO interfaces of varying thicknesses were prepared by pulsed laser deposition (PLD) on (001)-oriented STO substrates with uniform TiO_2 termination. The crystalline samples were grown at 730 °C at high oxygen pressure (1×10^{-2} mbar) to minimize the formation of oxygen vacancies, and then slowly cooled in the process gas. The observation of reflected-high-energy-electron (RHEED) oscillations during the growth allowed both the control of the LAO layer thickness, t_{LAO}, and the calibration of the growth rate. The amorphous samples were then grown at ambient temperature in 1×10^{-5} mbar of oxygen atmosphere. We assumed that the growth rate of such samples was the same as that of crystalline samples. Therefore, we controlled their nominal thickness by counting the laser shots during the growth and reported it in equivalent unit cells (euc), being 1 euc $\approx$ 0.38 nm. The correctness of this procedure was also verified by resorting to x-ray grazing incidence reflectometry to measure t_{LAO} in a few selected samples.

For the optical investigation, laser pulses of $\approx$35 fs and wavelength of 800 nm (1.55 eV photon energy) were generated at 1 kHz by a Ti:sapphire laser. Both the input fundamental and the output SHG beam are linearly polarized. In the following, the labels P, S, and D denote linear polarizations parallel, perpendicular, or at 45° with respect to the plane of incidence of light. In accordance with the four-fold rotational symmetry of the interface, we measured the only three independent non-vanishing SHG components: P-in P-out (PP), S-in P-out (SP), and D-in S-out (DS).[21]

In Fig. 1, we show the sheet conductance and the SHG intensity as a function of t_{LAO}. We observe that both the sheet conductance and the SHG intensity increase as a function of t_{LAO}. The conductance behavior is in qualitative agreement with the one previously reported for *a*-LAO/STO.[12] For comparison, in Fig. 1 we also report the SHG signal (filled stars) and the conductance (blue open star) measured for a *c*-LAO/STO sample with $t_{LAO} = 10$ euc. From this comparison, it is evident that the SHG signal at this LAO thickness is the same for both types of interfaces. We note that *c*-LAO/STO interfaces show approximately a saturation of the SHG signal above the conductance threshold (corresponding to four unit cells).[16] This is also evident in Fig. 1 for the *a*-LAO/STO interfaces above $t_{LAO} = 7$ euc. Therefore, we conclude that the SHG intensity is similar for all the *a*-LAO/STO interfaces lying in the saturation interval and, for these, to all the *c*-LAO/STO interfaces above the conductance threshold.

The oxygen vacancies that form at the *a*-LAO/STO interfaces during sample fabrication may be refilled by suitable post-annealing in oxygen. In order to demonstrate the effect of such process on the sheet conductance and on SHG,

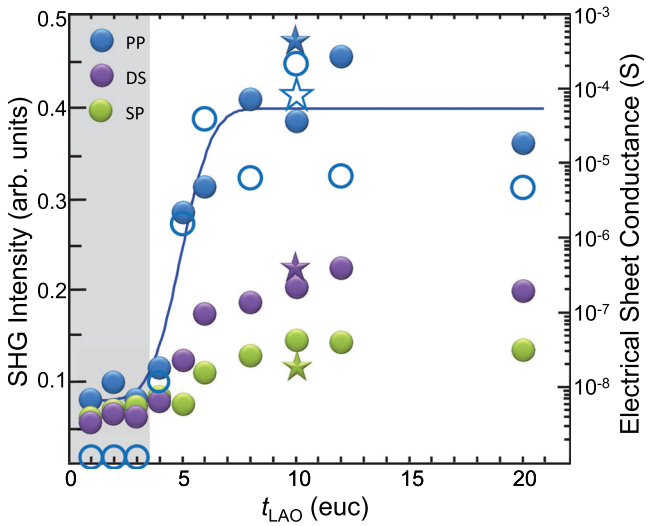

FIG. 1. SHG intensity (left-axis) and conductance (right-axis) for *a*-LAO/STO interfaces as a function of thickness. The SHG signal is indicated with filled circles for all ω-2ω polarization combinations: PP (blue), DS (violet), and SP (green). The conductivity values of the *a*-LAO/STO interfaces are indicated with open circles. The gray area encloses those samples whose conductance is below the detection limit. For comparison, we report the SHG signal (filled stars) and conductivity (blue open star) for a *c*-LAO/STO sample with a thickness of 10 euc. The solid line is a guide for eyes.

we performed measurements during such thermal treatments. In the following, we focus our attention on two samples with $t_{LAO} = 10$ euc and on a STO single crystal that was used as reference. These samples were heated in air from room temperature up to about 350 °C and then cooled back to room temperature.

The results of the conductivity measurements are reported in Fig. 2. The filled symbols refer to measurements taken during the heating stage, while the blue open symbols refer to measurements performed during the cooling stage. The STO single crystal shows a thermally activated behavior, typical of a wide band-gap insulator, with a conductance

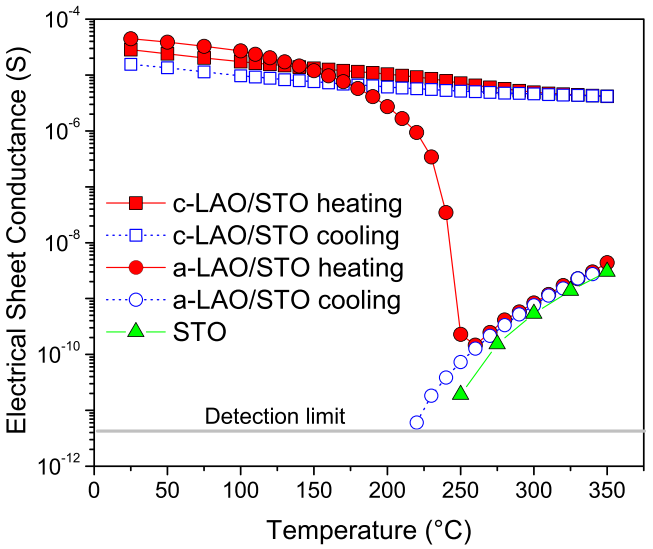

FIG. 2. Sheet conductance for the two *a*- and *c*-LAO/STO samples with 10 euc as a function of temperature. The red filled points refer to measurements taken while heating the sample in air from room temperature till 350 °C. Conversely, the blue open symbols refer to measurements performed by cooling samples back to room temperature. Green triangles refer to conductivity for bare STO used as reference.

falling below the detection limit under 250 °C.[27] The *c*-LAO/STO sample shows a typical metallic slope as a function of temperature. Such metallic behavior is unaffected by the annealing performed in oxidizing conditions, but the conductance value shows a slight decrease at the end of the thermal process.[25] The *a*-LAO/STO sample shows a rapid and irreversible decrease of conductance during the heating stage. The sample conductance intersects the STO curve at about 250 °C and follows the same behavior of STO during the remaining heating and cooling steps.

The results of the SHG measurements are reported in Fig. 3. They confirm that the doping mechanisms inducing the interfacial polarity sensed by SHG are quite different in the two material systems. For the *c*-LAO/STO sample, the behavior of the SHG signal as a function of temperature, for all the polarization combinations, is qualitatively the same of that observed for conductivity. The SHG signal is approximately constant during both the heating and cooling stages. After the cooling step, the SHG signal from the *c*-LAO/STO interface recovers approximately its initial room-temperature value. Conversely, in the case of the *a*-LAO/STO, we observe an overall decrease of the SHG signal as a function of temperature, analogous to the decrease of conductivity. However, SHG also shows a few significant features that are not visible in the conductivity measurements.

We notice that the decrease of the SHG signal starts already at about 110 °C, where we paused our temperature scan

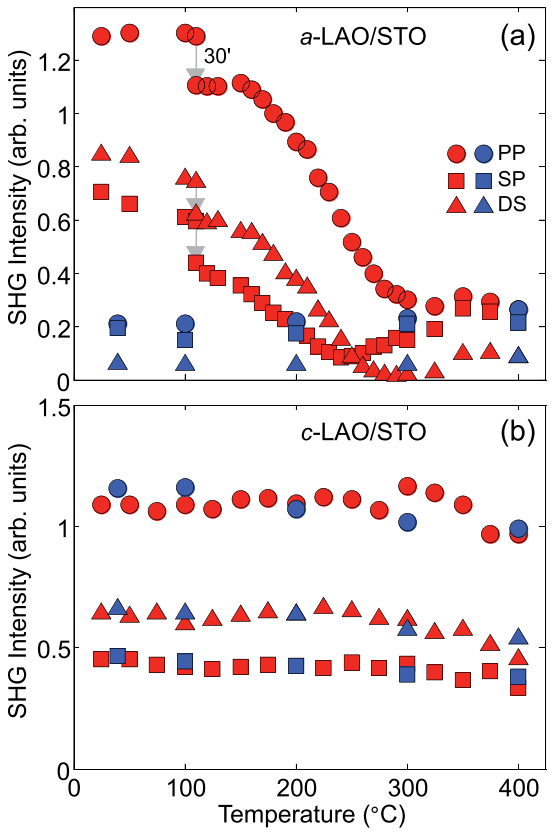

FIG. 3. SHG intensity as a function of temperature for 10 euc thick *a*- and *c*-LAO/STO samples (panel (a) and (b), respectively), for three polarization combinations: PP (circles), DS (triangles), ad SP (squares). Red (blue) points refer to the heating (cooling) stage. The arrow at 110 °C indicates the beginning of the SHG signal decrease. At this temperature, we waited for 30 min (30′ label in the figure) before continuing the temperature scan.

for 30 min. At this temperature, the SHG signal decreases continuously with an approximate rate of −30% per hour. After this break, we resumed increasing the temperature by 10 °C every five minutes. The SHG intensity shows a general decrease during the heating stage, with clear differences for the different polarization combinations. In particular, the DS signal decreases more rapidly than the SP one, till vanishing at about 300 °C. In contrast, the other two polarization combinations never become zero. The consequence of these different behaviors is that the SP and DS signals cross at about 250 °C. Therefore, below this temperature, DS is always higher than SP, while this relation is inverted above 250 °C. Above 320 °C, the DS signal slightly increases again. A similar increase is observed for the SP signal, which, after reaching its minimum at 250 °C, becomes equal to PP.

Finally, during the cooling process, the SHG signal for all the polarization combinations remains constant at the values reached for the highest temperatures. In particular, the SHG signal does not recover its initial room-temperature value. Moreover, the DS signal remains lower than that of SP, thus inverting the initial signal hierarchy of these two polarization combinations. This result shows that the obtained insulating interface is optically different from the untreated single crystal STO surface since the latter generates a SP signal that is always lower than the DS one, as long as the SHG photon energy is not close to the optical resonances of STO.[22]

Our measurements provide clear indications of irreversible chemical transformations taking place in our samples during annealing. In the case of *a*-LAO/STO, it is evident that the donor oxygen vacancies recombine with oxygen from the environment during the heating stage at about 250 °C. After this moment, the interface is electrically similar to single crystal STO, with no more role played by the interface in defining its electric transport properties. The *c*-LAO/STO sample only goes through some minor irreversible transformation that weakly affects its transport properties and is not probed, within the sensitivity of our measurements, by SHG. Such a slight decrease of conductivity in crystalline samples has also been often attributed to the neutralization of a residual amount of oxygen vacancies.[25] We observe that, if this is the case, the refilling of oxygen vacancies takes place at surprisingly different temperatures in the two kinds of interfaces.

The different evolution of the SHG and of the electric conductance under a thermal treatment clearly points to two different donor mechanisms in the *a*- and *c*-LAO/STO interfaces: oxygen vacancies in the first case and electronic reconstruction driven by interfacial polar discontinuity (possibly accompanied by residual oxygen vacancies) in the second case. Besides, for all the *c*- and *a*-LAO/STO heterostructures lying in the saturation interval, we observe a similar SHG signal.

As already demonstrated, SHG indirectly probes the charges and their spatial distribution at the interface.[20,22] When a space-charge region is created at the interface, this develops an electric field, $E_{polar}(z)$, that polarizes the electronic orbitals involved in the SHG process. This contribution is accounted in Eq. (1) by the $\hat{\chi}^{(3)}$ tensor. If we assume in that equation that $\hat{\chi}^{(2)} \ll \hat{\chi}^{(3)}$ and that $\hat{\chi}^{(3)}$ is

approximately constant over d_{polar}, the quantity χ^{eff} assumes a notable physical meaning, being proportional to the depth of the potential well induced by the charge distribution at the interface

$$\chi^{\text{eff}}_{\text{in,out}} \propto \chi^{(3)} \int E_{polar}(z)dz = \chi^{(3)} V_{well}, \tag{2}$$

where for simplicity, we have left out tensor indices, and V_{well} indicates the depth of the potential well. An estimate of V_{well} as a function of t_{LAO} is given in Fig. 4(a) for both *a*-LAO/STO and *c*-LAO/STO interfaces. The values shown in figure are obtained by averaging the square root of the SHG intensity over the measured polarization combinations. From Fig. 4(a), the similarity of V_{well} for all the samples above about 7 euc is evident. Again we note that *c*-LAO/STO interfaces show approximately a saturation of the SHG intensity above the conductance threshold. Therefore, we conclude that all the crystalline samples above the conductance threshold have an interfacial V_{well} similar to the amorphous samples in the saturation region. This result points to the existence of an universal depth of the interfacial potential well, despite the fundamentally different doping mechanism acting in these two material systems.

A possible microscopic scenario for the case of the *a*-LAO/STO interface, which might help explaining this similarity, is based on the assumption that a δ-doping mechanism caused by oxygen vacancies takes place at the *a*-LAO/STO interface.[28] The band diagram of *a*-LAO/STO would be therefore determined by the combination of two basic elements, that is the typical "dip" of the bands formed in the proximity of a δ-doping sheet[29] and the well known mismatch of the conduction bands of LAO and STO, making the states on the LAO side of the δ-doped interface unaccessible to the electronic wavefunctions. The interplay of these two components would lead to a band diagram such as that in Fig. 4(c), showing significant similarities, on the STO side, to the one foreseen by the electronic-reconstruction model for the *c*-LAO/STO case, as reported in Fig. 4(b). However, the fact that the potential-well depth in the *a*-LAO/STO and *c*-LAO/STO cases is about the same remains unexplained in this model. A possible explanation is that this depth is actually dominated by the difference between the conduction-band minimum energy in the STO bulk and the Fermi level, difference which is expected to be largely independent of the interface properties. We also notice that for a fixed shape of the potential well, the well depth should be proportional to both the amount of trapped electronic charge per unit area and to the penetration length of this charge in the STO bulk.

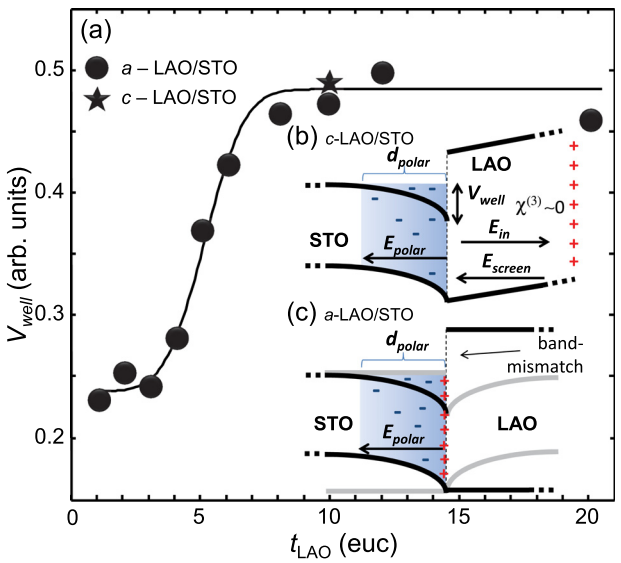

FIG. 4. In the main panel, the potential-well depth V_{well} for *a*-LAO/STO (circles) and *c*-LAO/STO (star) determined from SHG is reported as a function of t_{LAO}. The solid line is only a guide for eyes. In the insets (b) and (c), the possible band diagrams of a *c*-LAO/STO and *a*-LAO/STO interface are depicted. For the *c*-LAO/STO interface, the bending of the LAO bands is due to the built-in electric field, $\boldsymbol{E}_{\text{in}}$, as predicted by the *polar catastrophe* model. At the critical thickness, this field is compensated by $\boldsymbol{E}_{screen}$. The band structure of the *a*-LAO/STO interface is tentatively represented as a typical potential well derived from δ-doping, whose electronic states on the LAO side (depicted by gray wings) are made unaccessible by the LAO/STO band mismatch. The latter is highlighted by the gray lines on the STO side, showing its band structure in absence of δ-doping.

In conclusion we showed that, in all the *a*- and *c*-LAO/STO heterostructures above a given threshold, the electrons present at the interface are confined in a potential-well with a similar depth, independently of the specific doping mechanism. This leads to the observation of the existence of a fundamental mechanism for the formation of such interfacial potential.

We acknowledge funding from the European Union (Programme FP7/2007-2013, Grant Agreement No. 264098-MAMA; FP7-PEOPLE-2012-CIG, Grant Agreement No. PCIG12-GA-2012-326499-FOXIDUET), and Ministero dell'Istruzione, dell'Università e della Ricerca (PRIN 2010-11-OXIDE). D.P. is also grateful to N. Pryds and Y. Z. Chen for invaluable discussions.

[1]A. Ohtomo and H. Hwang, Nature **427**, 423 (2004).
[2]F. M. Granozio, G. Koster, and G. Rijnders, MRS Bull. **38**, 1017–1023 (2013).
[3]N. Nakagawa, H. Y. Hwang, and D. A. Muller, Nature Mater. **5**, 204 (2006).
[4]S. Thiel, G. Hammerl, A. Schmehl, C. Schneider, and J. Mannhart, Science **313**, 1942 (2006).
[5]M. L. Reinle-Schmitt, C. Cancellieri, D. Li, D. Fontaine, M. Medarde, E. Pomjakushina, C. W. Schneider, S. Gariglio, P. Ghosez, J. M. Triscone, and P. R. Willmott, Nat. Commun. **3**, 932 (2012).
[6]C. Cancellieri, D. Fontaine, S. Gariglio, N. Reyren, A. D. Caviglia, A. Fete, S. J. Leake, S. A. Pauli, P. R. Willmott, M. Stengel, P. Ghosez, and J. M. Triscone, Phys. Rev. Lett. **107**, 056102 (2011).
[7]C. Cantoni, J. Gazquez, F. Miletto Granozio, M. P. Oxley, M. Varela, A. R. Lupini, S. J. Pennycook, C. Aruta, U. Scotti di Uccio, P. Perna, and D. Maccariello, Adv. Mater. **24**, 3952 (2012).
[8]S. A. Pauli and P. R. Willmott, J. Phys. Condens. Matter **20**, 264012 (2008).
[9]K. Yoshimatsu, R. Yasuhara, H. Kumigashira, and M. Oshima, Phys. Rev. Lett. **101**, 026802 (2008).
[10]A. S. Kalabukhov, Y. A. Boikov, I. T. Serenkov, V. I. Sakharov, V. N. Popok, R. Gunnarsson, J. Borjesson, N. Ljustina, E. Olsson, D. Winkler, and T. Claeson, Phys. Rev. Lett. **103**, 146101 (2009).
[11]S. A. Chambers, M. H. Engelhard, V. Shutthanandan, Z. Zhu, T. C. Droubay, L. Qiao, P. V. Sushko, T. Feng, H. D. Lee, T. Gustafsson, E. Garfunkel, A. B. Shah, J.-M. Zuo, and Q. M. Ramasse, Surf. Sci. Rep. **65**, 317 (2010).
[12]Y. Z. Chen, N. Pryds, J. E. Kleibeuker, G. Koster, J. R. Sun, E. Stamate, B. G. Shen, G. Rijnders, and S. Linderoth, Nano Lett. **11**, 3774–3778 (2011).

[13]S. W. Lee, Y. Q. Liu, J. Heo, and R. G. Gordon, Nano Lett. **12**, 4775–4783 (2012).
[14]F. Trier, S. Amoruso, D. V. Christensen, A. Sambri, Y. Z. Chen, X. Wang, E. Stamate, R. Bruzzese, and N. Pryds, Appl. Phys. Lett. **103**, 031607 (2013).
[15]Z. Q. Liu, C. J. Li, W. M. Lü, X. H. Huang, Z. Huang, S. W. Zeng, X. P. Qiu, L. S. Huang, A. Annadi, J. S. Chen, J. M. D. Coey, T. Venkatesan, and Ariando, Phys. Rev. X **3**, 021010 (2013).
[16]A. Savoia, D. Paparo, P. Perna, Z. Ristic, M. Salluzzo, F. Miletto Granozio, U. Scotti di Uccio, C. Richter, S. Thiel, J. Mannhart, and L. Marrucci, Phys. Rev. B **80**, 075110 (2009).
[17]N. Ogawa, K. Miyano, M. Hosoda, T. Higuchi, C. Bell, Y. Hikita, and H. Y. Hwang, Phys. Rev. B **80**, 081106 (2009).
[18]A. Rubano, M. Fiebig, D. Paparo, A. Marino, D. Maccariello, U. Scotti di Uccio, F. Miletto Granozio, L. Marrucci, C. Richter, S. Paetel, and J. Mannhart, Phys. Rev. B **83**, 155405 (2011).
[19]T. Günter, A. Rubano, D. Paparo, M. Lilienblum, L. Marrucci, F. Miletto Granozio, U. Scotti di Uccio, R. Jany, C. Richter, J. Mannhart, and M. Fiebig, Phys. Rev. B **86**, 235418 (2012).
[20]A. Rubano, T. Günter, T. Fink, D. Paparo, L. Marrucci, C. Cancellieri, S. Gariglio, J.-M. Triscone, and M. Fiebig, Phys. Rev. B **88**, 035405 (2013).
[21]D. Paparo, A. Rubano, and L. Marrucci, J. Opt. Soc. Am. B **30**, 2452–2460 (2013).
[22]A. Rubano, C. Aruta, U. S. di Uccio, F. M. Granozio, L. Marrucci, T. Günter, T. Fink, M. Fiebig, and D. Paparo, Phys. Rev. B **88**, 245434 (2013).
[23]P. Godefroy, W. de Jong, C. W. van Hasselt, M. A. C. Devillers, and Th. Rasing, Appl. Phys. Lett. **68**(14), 1981–1983 (1996).
[24]For simplicity, in Eq. (1), we have omitted the Fresnel transformation matrices accounting for the propagation from/to the outside of the medium to/from the interfacial polar layer. An explicit expression for that may be found in Ref. 21.
[25]W. Siemons, G. Koster, H. Yamamoto, W. A. Harrison, G. Lucovsky, T. H. Geballe, D. H. A. Blank, and M. R. Beasley, Phys. Rev. Lett. **98**, 196802 (2007).
[26]C. Ohlhoff, G. Lüpke, C. Meyer, and H. Kurz, Phys. Rev. B **55**, 4596 (1997).
[27]A. Rubano, D. Paparo, F. Miletto Granozio, U. Scotti di Uccio, and L. Marrucci, J. Appl. Phys. **106**, 103515 (2009).
[28]This hypothesis is quite plausible, since oxygen is removed from STO as a consequence of an interface red-ox reaction,[12] which directly affects the terminating TiO_2 plane of STO. It is reasonable to assume that during the room temperature deposition process employed for *a*-LAO/STO growth, oxygen diffusivity is suppressed, so that interface vacancies do not redistribute within the bulk of STO.
[29]E. F. Schubert, J. Vac. Sci. Technol. A **8**, 2980–2996 (1990).